Late-stage volatile saturation as a potential trigger for explosive volcanic eruptions

Michael J. Stock*[1], Madeleine C.S. Humphreys[2], Victoria C. Smith[3], Roberto Isaia[4], David M. Pyle[1]

[1]Department of Earth Sciences, University of Oxford, South Parks Road, Oxford, OX1 3AN, UK

[2]Department of Earth Sciences, Durham University, Science Labs, Durham, DH1 3LE, UK

[3]Research Laboratory for Archaeology and the History of Art, University of Oxford, South Parks Road, Oxford, OX1 3QY, UK

[4]Istituto Nazionale di Geofisica e Vulcanologia, Osservatorio Vesuviano, via Diocleziano 328, 80124 Napoli, Italy

*E-mail: mike.stock@earth.ox.ac.uk

Magma reservoirs are thought to grow relatively slowly, assembling incrementally under volatile-saturated conditions. Eruptions may be triggered by injections of volatile-rich melt, or generation of over-pressure due to protracted crystallization. Here, we analyse fluorine, chlorine and water in apatite crystals trapped at different stages of magma evolution, and in melt inclusions from clinopyroxene and biotite crystals expelled during an explosive eruption of the Campi Flegrei caldera, Italy, about 4,000 years ago. We combine our geochemical analyses with thermodynamic modelling to reconstruct the evolution of magmatic volatile contents leading up to the explosive eruption. We find that the magma reservoir remained persistently water-undersaturated throughout most of its lifetime. Even crystals in contact with the melt shortly before eruption show that the magma was volatile-undersaturated. Our models suggest that the melt reached volatile saturation at low temperatures, just before

eruption. We suggest that late-stage volatile saturation probably triggered the eruption, and conclude that 'priming' of the magma system for eruption may occur on timescales much shorter than the decadal to centennial timescales thought typical for magma reservoir assembly. Thus, surface deformation pulses that record magma assembly at depth beneath Campi Flegrei and other similar magmatic systems may not be immediately followed by an eruption; and explosive eruptions may begin with little warning.

Volcanic gases (principally H_2O and CO_2) dissolved in silicate melts exert a first-order control on the eruptive behaviour of many volcanoes[1, 2, 3]. Vapour saturation in magmas may be reached during ascent[1, 4] or through progressive crystallization[5, 6]. After volatile saturation, continued growth of vapour bubbles during crystallization[5, 6] or replenishment[7, 8] will pressurize the magma reservoir, and may eventually trigger eruption. Constraining pre-eruptive volatile concentrations and the timing of volatile saturation is therefore critical to our understanding of volcanic eruptions. Although many models assume that saturation occurs early in magmatic evolution (for example, refs 1,9,10,11), it is not known whether this is generally the case; or whether, instead, melts can remain undersaturated on long timescales during crustal storage. Developing ways to constrain variations in dissolved magmatic volatile contents through time, in the build-up to an explosive eruption, would be invaluable for the assessment of volcanic hazards, as past eruptions provide clues to the future behaviour of the system.

Apatite, $Ca_5(PO_4)_3(F, Cl, OH)$, is a common accessory phase in igneous rocks that takes all major magmatic volatiles (OH, C, S, Cl, F) into its crystal structure. It has recently been used to elucidate the volatile contents of silicate melts in terrestrial[12, 13, 14] and extraterrestrial[15, 16] environments. Apatite offers several important benefits for the determination of pre-eruptive magmatic volatile contents compared to the widely used 'melt inclusion' approach. In

particular, apatites are less susceptible to post-entrapment volatile leakage, or to modification by post-entrapment crystallization or bubble growth[17]. Here, we present analyses of apatites and melt inclusions that are hosted in phenocryst phases (clinopyroxene and biotite) and were trapped and isolated from the melt at different times during the crystallization history of an evolving magma. We also analysed apatite microphenocrysts that remained in contact with the melt until shortly before eruption; and matrix glasses, which quenched during eruption. Combined with thermodynamic models, these 'texturally constrained' hydrous phases reveal how magmatic volatiles evolved (Fig. 1) in the build-up to the phonolitic Astroni 1 eruption, 4.3–4.1 kyr ago (ref. 18) (sample description in Supplementary Materials). The Astroni 1 eruption marked the beginning of the most recent phase of prolonged explosive volcanism at Campi Flegrei, one of the most hazardous volcanoes in Europe[18]. Our approach is distinct from previous studies, which have assessed apatite growth zoning[13] or texturally unconstrained analyses[12]. Although we focus on a single event, our approach can be applied widely to determine the temporal evolution of pre-eruptive volatiles in other volcanic systems.

Volatile variations in apatite and hydrous glasses

The volatile composition of apatite relates to that of its host liquid by a set of exchange reactions between F, Cl and OH, for example:

$$K_{(P,T)} = \frac{f_{H_2O}^{l}}{f_{HF}^{l}} \cdot \frac{X_F^{Ap}}{X_{OH}^{Ap}} \quad (1)$$

where exchange coefficients, K, are constant at a given pressure (P) and temperature (T) (ref. 12), f is fugacity, X is mole fraction and superscripts l and Ap denote the liquid and apatite phases, respectively. We measured F, Cl and OH directly using secondary ion mass spectrometry and electron microprobe analysis (see Supplementary Methods). We neglect

sulphur, because S diffusion in apatite is inhibited by a coupled substitution[19], and equilibrium is not maintained on short timescales. Apatite compositions from Astroni 1 show a negative correlation between X_F and X_{OH} and a weaker negative correlation between X_{Cl} and X_{OH} (where X_F, X_{Cl} and X_{OH} are the mole fractions of F, Cl and OH, respectively; Supplementary Table 1), demonstrating this exchange of components within the crystal volatile site. Some crystals are slightly non-stoichiometric, within the range reported in other studies[20]. We focus on mole fraction ratios as these relate to liquid composition, pressure and temperature through relationships such as equation (1). Data show a positive correlation between X_{Cl}/X_{OH} and X_F/X_{OH} (Fig. 2a), with one low-X_{Cl}, high-X_F outlier. In general, X_F/X_{Cl} is constant within error, except in the outlier which has high X_F/X_{Cl} (Fig. 2b). Clinopyroxene-hosted apatite inclusions extend to higher $X_{halogen}/X_{OH}$ ratios than biotite-hosted apatite inclusions. Both clinopyroxene- and biotite-hosted inclusions extend to higher $X_{halogen}/X_{OH}$ ratios than apatite microphenocrysts that were in contact with melt until eruption. The overall $X_{halogen}/X_{OH}$ trend is apparently linear, suggesting that there was no significant relative change in F or Cl compatibility during apatite crystallization.

Melt inclusions are typically phonolitic, with an average molar $Na_2O/(Na_2O + K_2O)$ of 0.44 and $Al_2O_3/(CaO + Na_2O + K_2O)$ of 0.87, similar to Vesuvian melt compositions[21]. MgO and FeO concentrations are <0.78 wt% and <4.20 wt%, respectively (Supplementary Table 2). Fluorine and Cl contents of clinopyroxene- and biotite-hosted melt inclusions correlate negatively with MgO (Fig. 3a, b), reflecting halogen incompatibility in the silicate melt during fractionation. Water is constant within error in clinopyroxene-hosted melt inclusions (~2 wt%), but is highly variable in biotite-hosted inclusions (1.3–4.5 wt%), with no correlation between melt inclusion H_2O and MgO (Fig. 3d). All melt inclusions contain very low CO_2 contents, typically <250 ppm (Supplementary Table 2), similar to concentrations observed in other Campi Flegrei magmas[9, 22].

Matrix glasses have MgO contents similar to the most evolved melt inclusions. Fluorine and Cl contents are similar to those of biotite-hosted melt inclusions and the most evolved clinopyroxene-hosted inclusions (Fig. 3a–c). However, matrix glasses have low H_2O contents relative to both clinopyroxene- and biotite-hosted melt inclusions, typically <1 wt% (Fig. 3d).

Modelling fractionation and volatile saturation

We model magma evolution in the Campi Flegrei system using the Rhyolite-MELTS thermodynamic software[23, 24, 25, 26] (details in Supplementary Discussion). Because major and trace element trends between different eruptions of Campi Flegrei can be related by fractional crystallization of a single parental magma[27], we use the most primitive olivine-hosted melt inclusion reported from the past 15 kyr (Mi1-C1-o5-M1 of ref. 28) as the starting composition. Models were run over the pressure range 50–300 MPa, at an oxygen fugacity 1 log unit above the Quartz-Fayalite-Magnetite buffer (f_{O2} = QFM + 1) and with liquidus H_2O concentrations (L_{H2O}) of 2–3 wt%, to simulate the entire range of conditions identified in previous phase equilibria and petrological studies as best reproducing the stable phase assemblages observed in Campi Flegrei eruptions[24, 25, 26]. Because Rhyolite-MELTS uses a pure-H_2O solubility model that is not appropriate for alkali melts (see Supplementary Discussion), we repressed fluid exsolution in our models and instead used recent experimental data as a guide to volatile saturation in Campi Flegrei magmas (Fig. 4).

The model results confirm the crystallization sequence: olivine (~1,330 °C) + clinopyroxene (~1,080 °C) + apatite (~1,020 °C) + biotite (~910 °C) + K-feldspar (~790 °C) at 150 MPa, L_{H2O} = 3 wt% (Fig. 4). This matches the observed phase assemblage in Astroni 1 products, except that olivine is absent in natural samples and fluorite occurs as a late microphenocryst phase. Within the modelled range, L_{H2O} has no effect on the order of crystallization, but clinopyroxene and apatite both arrive on the liquidus at slightly higher temperatures at lower

L_{H2O} conditions (ΔT ~ 20 °C and ~30 °C, respectively). During fractionation, modelled melt MgO contents decrease from ~3.8 wt% at *clinopyroxene-in* to ~0.2 wt% at *K-feldspar-in*; dissolved H_2O contents increase from 3.7 wt% to 6.2 wt% over the same interval. Pressure has little effect on the modelled down-temperature MgO and H_2O evolution of the system before volatile saturation is achieved, but would change L_{H2O} if volatile saturation occurred before *olivine-in* (Fig. 4).

Magma storage pressures can be constrained independently from geophysical observations. Seismic reflection data suggest that the main melt zone beneath Campi Flegrei is at ~7–7.5 km (refs 29,30), with ephemeral sills and intrusions extending to ~3 km (refs 30,31). This equates to pressures of 170–180 MPa for the main reservoir, assuming a melt density of 2,440 kg m^{-3}. The H_2O solubility of phonolitic melts is >7.5 wt% at 900–950 °C, 200 MPa (ref. 21), falling to ~6.33 wt% H_2O at 870 °C, 150 MPa and <3 wt% H_2O at <50 MPa (ref. 32). On the basis of these experimental data, H_2O saturation in our model runs is achieved at 750–785 °C at 200 MPa and 775–805 °C at 150 MPa, within the range L_{H2O} = 2–3 wt% (Fig. 4). In both cases this is significantly later than *apatite-in*.

Progressive temporal trends in melt volatile contents

The modelled crystallization sequence provides the context for us to interpret progressive changes in melt and apatite volatile compositions, from clinopyroxene-hosted melt or apatite inclusions, to biotite-hosted inclusions, to microphenocrysts and matrix glasses.

Apatite–liquid exchange coefficients (equation (1)) have been constrained experimentally for the system apatite-fluid as a function of pressure and temperature (ref. 12 and references therein). At constant liquid volatile composition, decreasing temperature causes a strong increase in apatite $X_{halogen}/X_{OH}$ ratios (Fig. 2a). However, the pressure dependence is small and almost exclusively affects X_{Cl}/X_{OH} (ref. 12). The trend of decreasing X_{Cl}/X_{OH} and X_F/X_{OH}

during magmatic evolution revealed by our data set is inconsistent with changing K due to cooling or depressurization (Fig. 2a; see Supplementary Discussion for model details). Although magma mixing may cause temporary heating, interpretations involving significant long-term heating or pressurization are not geologically realistic during the protracted magmatic fractionation required to produce the Astroni 1 phenocryst assemblage (Fig. 4). Instead, the observed trend in apatite compositions reflects a progressive change in the melt volatile composition through time, during magma evolution.

Within the limits of analytical precision, melt inclusions show that melt halogen concentrations increased during magma evolution (Fig. 3a–c). Assuming that K_D (equation (1)) does not vary significantly with evolving melt composition, the decreasing apatite $X_{halogen}/X_{OH}$ ratios (Fig. 2) must reflect a comparative increase in dissolved melt H_2O contents during crystallization: that is, H_2O-undersaturated behaviour. This concurs with our Rhyolite-MELTS modelling. When compared with phonolite solubility experiments[21, 32], models predict late, low-temperature H_2O saturation, with melt H_2O concentrations increasing throughout magmatic evolution, at pressures consistent with independent estimates of magma storage depths (that is, $P > 150$ MPa; Fig. 4).

Trends in apatite compositions observed in Astroni 1 can be reproduced using models based on volatile-undersaturated fractionation[33], assuming that F, Cl and H_2O are moderately incompatible during crystallization of apatite and biotite (insets Fig. 2 and Supplementary Discussion). The effect of biotite precipitation on apatite compositional evolution is minor[33], whereas the effect of late-stage vapour saturation on the compositional evolution of apatite is orders of magnitude more significant[33]. This is because vapour-melt Cl partition coefficients in H_2O-saturated phonolites are >1 (ref. 34); whereas F is retained within the silicate liquid[21]. The effect of this is to increase the F/Cl ratio in the melt. After vapour saturation, apatite will move towards a F–Cl binary composition, progressing towards endmember fluorapatite (case

2 of ref. 33; insets Fig. 2). We do not see this trend in our data set (Fig. 2), and infer that the system remained volatile-undersaturated while the apatite microphenocrysts were in equilibrium with the melt.

If the melt inclusions were trapped in the presence of a hydrosaline brine, we would expect to see constant melt Cl instead of the observed negative correlation between Cl and MgO (Fig. 3a). Experimental data show that in the presence of a vapour phase, Cl-solubility in phonolitic magmas is pressure dependent[34]. The highest Cl concentrations measured in Astroni 1 melt inclusions (>1 wt%) require unreasonably low entrapment pressures (<25 MPa) under vapour-saturated conditions[34]. Instead, our data are consistent with crystallization in the absence of a free fluid, in agreement with experimental constraints[35].

Melt inclusion halogen concentrations show a negative correlation with MgO (Fig. 3a, b), which is consistent with incompatible behaviour during crystallization. However, the lack of correlation between H_2O and MgO in melt inclusions (Fig. 3d) cannot be reconciled either with apatite compositions (Fig. 2) or crystallization models (Fig. 4). Instead, we suggest that H_2O contents of melt inclusions have been modified by diffusion after entrapment, whereas halogen concentrations record primary magmatic processes. Hydrogen diffuses rapidly through pyroxene, even at 800 °C (ref. 36), and this is widely implicated in post-entrapment modification of melt inclusion volatile contents[37]. From published H diffusivity data, the H_2O concentrations of clinopyroxene-hosted melt inclusions in the centre of mm-scale phenocrysts will change on timescales of hours[36]. Thus, short-term stalling of magma at shallow depths after volatile saturation provides a mechanism to reset the H_2O contents of melt inclusions with varying MgO concentrations. No data exist for H diffusivity in biotite, although the strong cleavage would presumably reduce its competency as a melt inclusion host. High H_2O concentrations in some biotite-hosted inclusions (Fig. 3d) suggest that melt H_2O contents could have reached >4.5 wt% during biotite crystallization. Biotite-hosted melt inclusions

with H_2O contents that approach the concentrations measured in matrix glass have probably leaked. The low H_2O content of matrix glass is consistent with efficient syn-eruptive degassing during magma ascent. Under equilibrium conditions at depth, Cl would partition preferentially into the vapour phase[34]. However, halogens diffuse significantly more slowly than H_2O in silicate melts[38], inhibiting vapour-melt equilibration and inducing disequilibrium on short timescales during ascent. Thus, degassed matrix glasses may retain Cl concentrations similar to evolved melt inclusions (Fig. 3). At low pressure, vapour-melt Cl partition coefficients approach unity[34].

Timescales of volatile undersaturation

If the magma became volatile-saturated before eruption this should result in disequilibrium between the melt and pre-existing apatite microphenocrysts. However, apatite volatile data show no evidence for partial re-equilibration towards strongly Cl-poor, F-rich (volatile-saturated) compositions as predicted by the model of ref. 33 (Fig. 2), even within 16 μm of the crystal rims (Supplementary Fig. 1). We can use diffusion constraints[39] to estimate the maximum time between volatile saturation and eruption. At 800 °C and 1 GPa, the characteristic timescale for halogen diffusion over ~16 μm is ~10 days. At 1 atm this time would be ~3 yr. This suggests that the maximum time delay between volatile saturation and eruption in Astroni 1 was of the order of $10–10^3$ days. Hence, the magma chamber remained persistently H_2O-undersaturated until only shortly before eruption. Similarly, the lack of evidence for syn-eruptive volatile loss from apatite microphenocrysts is due to the diffusive re-equilibration time exceeding realistic eruptive timescales.

Pre-eruptive volatile undersaturation at Campi Flegrei

In combination, analysis of apatites and melt inclusions offers great potential as a forensic petrological tool, providing new information about the temporal evolution of pre-eruptive

volatile contents in volcanic systems. Using this method, we have demonstrated that the Astroni 1 magma chamber remained H_2O-undersaturated until shortly before eruption. This interpretation is consistent with thermodynamic modelling of magma evolution (Fig. 4), and with interpretations of ongoing patterns of degassing and deformation in Campi Flegrei, which can be explained by local volatile saturation at the roof of a largely H_2O-undersaturated magma chamber[40]. We observe a measurable decrease in apatite $X_{halogen}/X_{OH}$ between biotite-hosted inclusions and microphenocrysts, indicating continued crystallization and an increase in melt H_2O concentration after *biotite-in*. Because H_2O saturation is predicted at temperatures only slightly lower than *biotite-in* (Fig. 4), but microphenocrysts have not re-equilibrated with a volatile-saturated melt, we suggest that the melt became H_2O-saturated just before eruption. In Astroni 1, only a small amount of additional crystallization is required to significantly increase the abundance of the aqueous vapour phase (Fig. 4), generating overpressures that would exceed the fracture criterion, inducing eruption[5] (Supplementary Fig. 2). We cannot discount the possibility that the pre-eruptive melt remained H_2O-undersaturated, and eruption was initiated by an external trigger; however, in the absence of any evidence for an external trigger, we suggest that progressive concentration of dissolved H_2O in the silicate melt triggered eruption after saturation was eventually achieved.

Because H_2O concentrations increase during crystallization, we infer that fresh batches of mafic melt arriving from depth would probably be more volatile-undersaturated than the evolved melts within an upper crustal reservoir. Although Astroni 1 shows no evidence of pre-eruptive magma mixing[18, 41], mingling is reported in other Campi Flegrei eruptions, including later eruptions from the Astroni vent[10, 18, 41]. The solubility of H_2O in phonolite is not significantly affected by temperature[42], so pre-eruptive magma replenishment and mixing would ‘dilute’ the dissolved volatile content of the silicate melt, returning the system to a

more undersaturated state. In this case, we expect the repose period between eruptions to reflect the balance between timescales of magma storage and crystallization (driving the system towards volatile saturation), and the recharge rate (driving it away). Volatile-undersaturated recharge would require greater crustal deformation than volatile-saturated mixing to accommodate new melt without exceeding the fracture criterion[43]. Such deformation may be responsible for observed large-scale inter-eruptive bradyseismicity at Campi Flegrei[44, 45], with recharge events inducing significant magma chamber dilation during repose periods.

Volcanological implications

Our data show that the sub-volcanic feeding systems for explosive eruptions can remain volatile-undersaturated until late in their evolution. This implies that the depths of magma stalling and storage are not controlled by changes in melt rheology resulting from degassing-induced crystallization[46], but may instead reflect local crustal discontinuities in density or rigidity[47]. Furthermore, melt inclusion H_2O–CO_2 data give only a minimum estimate of crystallization pressures.

The potential for persistent magmatic volatile undersaturation has significant implications for the monitoring of restless volcanoes. Although magma chamber assembly can occur on decadal timescales[48], there is a growing number of examples where deformation pulses are not immediately followed by eruption; and others, including the only historic eruption of Campi Flegrei[44], where explosive eruptions begin with little or no early geodetic 'warning'[49, 50]. This suggests that the final pre-eruptive 'priming' of the system may occur on timescales far shorter than timescales of assembly; perhaps as short as days to months. Because ground-deformation and seismic evidence for unrest may accompany the long-term processes of subterranean magma recharge and chamber assembly, and not simply pre-eruptive activity,

this poses a challenge for agencies engaged in volcano monitoring. This is not a ubiquitous triggering mechanism. However, in persistently volatile-undersaturated systems, the onset of volatile saturation might provide some pre-eruptive chemical indicators, such as accompanying the leakage of magmatic volatiles into the surrounding edifice, or hydrothermal system, and an increased magmatic component in fumarolic gases at the surface. Successful monitoring of these systems will demand high temporal resolution chemical and isotopic analysis of fluid and gas emissions[45].

Acknowledgements

This research was funded by a NERC studentship NE/K500811/01 awarded to M.J.S. and a NERC Edinburgh Ion Microprobe Facility grant (IMF519/0514). M.C.S.H. was supported by a Royal Society University Research Fellowship. M.C.S.H. and V.C.S. acknowledge funding from NERC grant NE/K003852/1. This work has benefited from discussion with R. Brooker, J. Riker and P. Candela. The review of W. Bohrson significantly improved the manuscript. We are grateful to R. Hinton and N. Charnley for assistance with SIMS and SEM analysis, respectively. We also thank D. Harlov for providing synthetic apatite standards for SIMS calibration and R. van Elsas for technical support during mineral separation.

Author Contributions

M.J.S., M.C.S.H. and V.C.S. conceived the project and analytical strategy. V.C.S. and R.I. collected samples, M.J.S. and V.C.S. performed the EPMA and SIMS analyses and M.J.S. and M.C.S.H. performed the modelling. M.J.S. analysed the data and wrote the first draft of the manuscript, which was revised by all authors.

Competing financial interests

The authors declare no competing financial interests.

Methods

A representative bulk sample of the Astroni 1 pyroclastic deposit was obtained from within the Campi Flegrei caldera in Naples, Italy. Clinopyroxene and biotite phenocrysts were picked and apatite microphenocrysts were separated using magnetic and heavy liquid separation techniques. All samples were mounted in epoxy resin, carbon coated and mapped using an FEI Quanta 650 FEG-scanning electron microscope (SEM) operating with a 20 kV and ~7 nA beam.

Major and trace elements were measured in apatites and hydrous glasses using a JEOL 8600 wavelength-dispersive electron microprobe (EPMA). Apatite analyses were collected with a 10 nA, 15 kV, defocused (5 μm diameter) beam and reduced halogen count times to limit the potential for halogen migration during irradiation[51, 52, 53]. Samples and standards were carbon coated together before analysis to ensure constant light-element X-ray attenuation. Glass analyses were collected using a 6 nA, 15 kV, defocussed (10 μm diameter) beam and short Na count times, to reduce alkali loss during irradiation[54]. Secondary standards were analysed to check the accuracy and reproducibility of results (Supplementary Table 3). Samples were re-polished after SEM and EPMA analysis, to remove any potential compositional modification resulting from electron-beam exposure[52].

Samples were gold coated and analysed for light-element isotopes using a Cameca IMS-4f ion microprobe, operating with a 10 keV $^{16}O^-$ primary ion beam. For apatite, spot analyses were made using a 5 nA beam for most analyses, which was reduced to 2.5 nA for smaller inclusions. To reduce any surface contamination, samples were pre-sputtered for ≥3 min before analysis, with a raster of 10–15 μm^2. Melt inclusion volatiles were measured in two separate analyses. In the first analysis, H_2O, F and light elements were measured using a 4 nA primary ion beam, with a ≥3 min pre-sputter over a 10 μm^2 area. The second analysis, for

CO_2 measurement, was made in the same spot, using a 4 nA beam and ≥2 min pre-sputter over a 15 μm^2 area. A field aperture was applied during melt inclusion analysis to further reduce contamination from the crater edges, limiting the measured secondary ions to the central ~8–10 μm in the first analyses and ~20 μm in the second analyses.

Working curves for apatite H_2O, F and Cl concentrations were produced using a range of natural and synthetic apatite standards, such as ^{1}H, ^{19}F or ^{35}Cl, normalized to ^{44}Ca (Supplementary Fig. 3). Equivalent working curves for glass H_2O and CO_2 concentrations were produced as ^{1}H or ^{12}C, normalized to ^{30}Si (Supplementary Figs 4 and 5). Fluorine and other trace elements were calibrated in glass analyses against NIST SRM610, with ^{44}Ca as an internal standard. Full method details are available in the Supplementary Information.

References

1 Roggensack, K., Hervig, R. L., McKnight, S. B. & Williams, S. N. Explosive Basaltic Volcanism from Cerro Negro Volcano: Influence of Volatiles on Eruptive Style. *Science* **277**, 1639-1642 (1997).

2 Wilson, L. Relationships between pressure, volatile content and ejecta velocity in three types of volcanic explosion. *J. Volc.and Geotherm. Res.* **8**, 297-313 (1980).

3 Huppert, H. E. & Woods, A. W. The role of volatiles in magma chamber dynamics. *Nature* **420**, 493-495 (2002).

4 Woods, A. W. & Koyaguchi, T. Transitions between explosive and effusive eruptions of silicic magmas. *Nature* **370**, 641-644 (1994).

5 Tait, S., Jaupart, C. & Vergniolle, S. Pressure, gas content and eruption periodicity of a shallow, crystallising magma chamber. *Earth Planet. Sci. Lett.* **92**, 107-123 (1989).

6 Blake, S. Volatile oversaturation during the evolution of silicic magma chambers as an eruption trigger. *J. Geophys. Res.* **89**, 8237-8244 (1984).

7 Folch, A. & Martí, J. The generation of overpressure in felsic magma chambers by replenishment. *Earth Planet. Sci. Lett.* **163**, 301-314 (1998).

8 Sparks, S. R. J., Sigurdsson, H. & Wilson, L. Magma mixing: a mechanism for triggering acid explosive eruptions. *Nature* **267**, 315-318 (1977).

9 Arienzo, I., Moretti, R., Civetta, L., Orsi, G. & Papale, P. The feeding system of Agnano–Monte Spina eruption (Campi Flegrei, Italy): dragging the past into present activity and future scenarios. *Chem. Geol.* **270**, 135-147 (2010).

10 Isaia, R., D'Antonio, M., Dell'Erba, F., Di Vito, M. & Orsi, G. The Astroni volcano: the only example of closely spaced eruptions in the same vent area during the recent history of the Campi Flegrei caldera (Italy). *J. Volc. Geotherm. Res.* **133**, 171-192 (2004).

11 Humphreys, M. C. S., Blundy, J. D. & Sparks, R. S. J. Shallow-level decompression crystallisation and deep magma supply at Shiveluch Volcano. *Contrib. Mineral. Petrol.* **155**, 45-61 (2008).

12 Piccoli, P. & Candela, P. Apatite in felsic rocks; a model for the estimation of initial halogen concentrations in the Bishop Tuff (Long Valley) and Tuolumne Intrusive Suite (Sierra Nevada Batholith) magmas. *Am. J. Sci.* **294**, 92-135 (1994).

13 Boyce, J. W. & Hervig, R. L. Magmatic degassing histories from apatite volatile stratigraphy. *Geology* **36**, 63-66 (2008).

14 Scott, J. A., Humphreys, M. C. S., Mather, T. A., Pyle, D. M. & Stock, M. J. Insights into the behaviour of S, F, and Cl at Santiaguito Volcano, Guatemala, from apatite and glass. *Lithos* **232**, 375-394 (2015).

15 McCubbin, F. M. *et al.* Fluorine and chlorine abundances in lunar apatite: Implications for heterogeneous distributions of magmatic volatiles in the lunar interior. *Geochim. Cosmochim. Acta* **75**, 5073-5093 (2011).

16 Boyce, J. W., Tomlinson, S. M., McCubbin, F. M., Greenwood, J. P. & Treiman, A. H. The lunar apatite paradox. *Science* **344**, 400-402 (2014).

17 Lowenstern, J. B. in *Magmas, Fluids, and Ore Deposits* (ed. Thompson, J. F. H.) 71–89 (Mineralogical Society of Canada, 1995).

18 Smith, V. C., Isaia, R. & Pearce, N. J. G. Tephrostratigraphy and glass compositions of post-15 kyr Campi Flegrei eruptions: implications for eruption history and chronostratigraphic markers. *Quat. Sci. Rev.* **30**, 3638-3660 (2011).

19 Peng, G., Luhr, J. F. & McGee, J. J. Factors controlling sulfur concentrations in volcanic apatite. *Am. Min.* **82**, 1210-1224 (1997).

20 Nadeau, S. L., Epstein, S. & Stolper, E. Hydrogen and carbon abundances and isotopic ratios in apatite from alkaline intrusive complexes, with a focus on carbonatites. *Geochim. Cosmochim. Acta* **63**, 1837-1851 (1999).

21 Webster, J. D., Goldoff, B., Sintoni, M. F., Shimizu, N. & De Vivo, B. C–O–H–Cl–S–F volatile solubilities, partitioning, and mixing in phonolitic–trachytic melts and aqueous–carbonic vapor±saline liquid at 200 MPa. *J. Petrol.* **55**, 2217-2248 (2014).

22 Marianelli, P., Sbrana, A. & Proto, M. Magma chamber of the Campi Flegrei supervolcano at the time of eruption of the Campanian Ignimbrite. *Geology* **34**, 937-940 (2006).

23 Gualda, G. A. R., Ghiorso, M. S., Lemons, R. V. & Carley, T. L. Rhyolite-MELTS: a modified calibration of MELTS optimized for silica-rich, fluid-bearing magmatic systems. *J. Petrol.* **53**, 875-890 (2012).

24 Fowler, S. J., Spera, F. J., Bohrson, W. A., Belkin, H. E. & De Vivo, B. Phase equilibria constraints on the chemical and physical evolution of the Campanian Ignimbrite. *J. Petrol.* **48**, 459-493 (2007).

25 Cannatelli, C. Understanding magma evolution at Campi Flegrei (Campania, Italy) volcanic complex using melt inclusions and phase equilibria. *Miner. Petrol.* **104**, 29-42 (2012).

26 Bohrson, W. A. *et al. Petrogenesis of the Campanian ignimbrite: implications for crystal-melt separation and open-system processes from major and trace elements and Th isotopic data* (Developments in Volcanology, Elsevier, New York, 2006).

27 Civetta, L., Carluccio, E., Innocenti, F., Sbrana, A. & Taddeucci, G. Magma chamber evolution under the Phlegraean Fields during the last 10 ka: trace element and isotop data. *Eur. J. Mineral.* **3**, 415-428 (1991).

28 Cannatelli, C. *et al.* Geochemistry of melt inclusions from the Fondo Riccio and Minopoli 1 eruptions at Campi Flegrei (Italy). *Chem. Geol.* **237**, 418-432 (2007).

29 Zollo, A. *et al.* Seismic reflections reveal a massive melt layer feeding Campi Flegrei caldera. *Geophys. Res. Lett.* **35** L12306 (2008).

30 De Siena, L., Del Pezzo, E. & Bianco, F. Seismic attenuation imaging of Campi Flegrei: Evidence of gas reservoirs, hydrothermal basins, and feeding systems. *J. Geophys. Res.* **115** B09312 (2010).

31 Woo, J. Y. L. & Kilburn, C. R. J. Intrusion and deformation at Campi Flegrei, southern Italy: sills, dikes, and regional extension. *J. Geophys. Res.* **115** B12210 (2010).

32 Carroll, M. R. & Blank, J. G. The solubility of H_2O in phonolitic melts. *Am. Min.* **82**, 549-556 (1997).

33 Candela, P. A. Toward a thermodynamic model for the halogens in magmatic systems: an application to melt-vapor-apatite equilibria. *Chem. Geol.* **57**, 289-301 (1986).

34 Signorelli, S. & Carroll, M. R. Solubility and fluid-melt partitioning of Cl in hydrous phonolitic melts. *Geochim. Cosmochim. Acta* **64**, 2851-2862 (2000).

35 Webster, J. D. & De Vivo, B. Experimental and modeled solubilities of chlorine in aluminosilicate melts, consequences of magma evolution, and implications for exsolution of hydrous chloride melt at Mt. Somma-Vesuvius. *Am. Min.* **87**, 1046-1061 (2002).

36 Woods, S. C., Mackwell, S. & Dyar, D. Hydrogen in diopside: diffusion profiles. *Am. Min.* **85**, 480-487 (2000).

37 Danyushevsky, L. V., McNeill, A. W. & Sobolev, A. V. Experimental and petrological studies of melt inclusions in phenocrysts from mantle-derived magmas: an overview of techniques, advantages and complications. *Chem. Geol.* **183**, 5-24 (2002).

38 Baker, D. R., Freda, C., Brooker, R. A. & Scarlato, P. Volatile diffusion in silicate melts and its effects on melt inclusions. *Ann. Geophys.* **48**, 699-717 (2005).

39 Brenan, J. Kinetics of fluorine, chlorine and hydroxyl exchange in fluorapatite. *Chem. Geol.* **110**, 195-210 (1993).

40 Bodnar, R. J. *et al.* Quantitative model for magma degassing and ground deformation (bradyseism) at Campi Flegrei, Italy: Implications for future eruptions. *Geology* **35**, 791-794 (2007).

41 Tonarini, S., D'Antonio, M., Di Vito, M. A., Orsi, G. & Carandente, A. Geochemical and B–Sr–Nd isotopic evidence for mingling and mixing processes in the magmatic system that fed the Astroni volcano (4.1–3.8 ka) within the Campi Flegrei caldera (southern Italy). *Lithos* **107**, 135-151 (2009).

42 Schmidt, B. C. & Behrens, H. Water solubility in phonolite melts: Influence of melt composition and temperature. *Chem. Geol.* **256**, 259-268 (2008).

43 Blake, S. Volcanism and the dynamics of open magma chambers. *Nature* **289**, 783-785 (1981).

44 Guidoboni, E. & Ciuccarelli, C. The Campi Flegrei caldera: historical revision and new data on seismic crises, bradyseisms, the Monte Nuovo eruption and ensuing earthquakes (twelfth century 1582 AD). *Bull. Volc.* **73**, 655-677 (2011).

45 Chiodini, G. *et al.* Evidence of thermal-driven processes triggering the 2005–2014 unrest at Campi Flegrei caldera. *Earth Planet. Sci. Lett.* **414**, 58-67 (2015).

46 Annen, C., Blundy, J. D. & Sparks, R. S. J. The genesis of intermediate and silicic magmas in deep crustal hot zones. *J. Pet.* **47**, 505-539 (2006).

47 Chaussard, E. & Amelung, F. Regional controls on magma ascent and storage in volcanic arcs. *Geochem., Geophys., Geosyst.* **15**, 1407-1418 (2014).

48 Druitt, T. H., Costa, F., Deloule, E., Dungan, M. & Scaillet, B. Decadal to monthly timescales of magma transfer and reservoir growth at a caldera volcano. *Nature* **482**, 77-80 (2012).

49 Biggs, J. *et al.* Global link between deformation and volcanic eruption quantified by satellite imagery. *Nat Commun.* **5**, 3471 (2014).

50 Parks, M. M. *et al.* Evolution of Santorini Volcano dominated by episodic and rapid fluxes of melt from depth. *Nat. Geosci.* **5**, 749-754 (2012).

51 Stormer Jr, J. C., Pierson, M. L. & Tacker, R. C. Variation of F and Cl X-ray intensity due to anisotropic diffusion in apatite. *Am. Min.* **78**, 641-648 (1993).

52 Stock, M. J., Humphreys, M. C. S., Smith, V. C., Johnson, R. D. & Pyle, D. M. New constraints on electron-beam induced halogen migration in apatite. *Am. Min.* **100**, 281-293 (2015).

53 Goldoff, B., Webster, J. D. & Harlov, D. E. Characterization of fluor-chlorapatites by electron probe microanalysis with a focus on time-dependent intensity variation of halogens. *Am. Min.* **97**, 1103-1115 (2012).

54 Humphreys, M. C. S., Kearns, S. L. & Blundy, J. D. SIMS investigation of electron-beam damage to hydrous, rhyolitic glasses: Implications for melt inclusion analysis. *Am. Min.* **91**, 667-679 (2006).

Figures

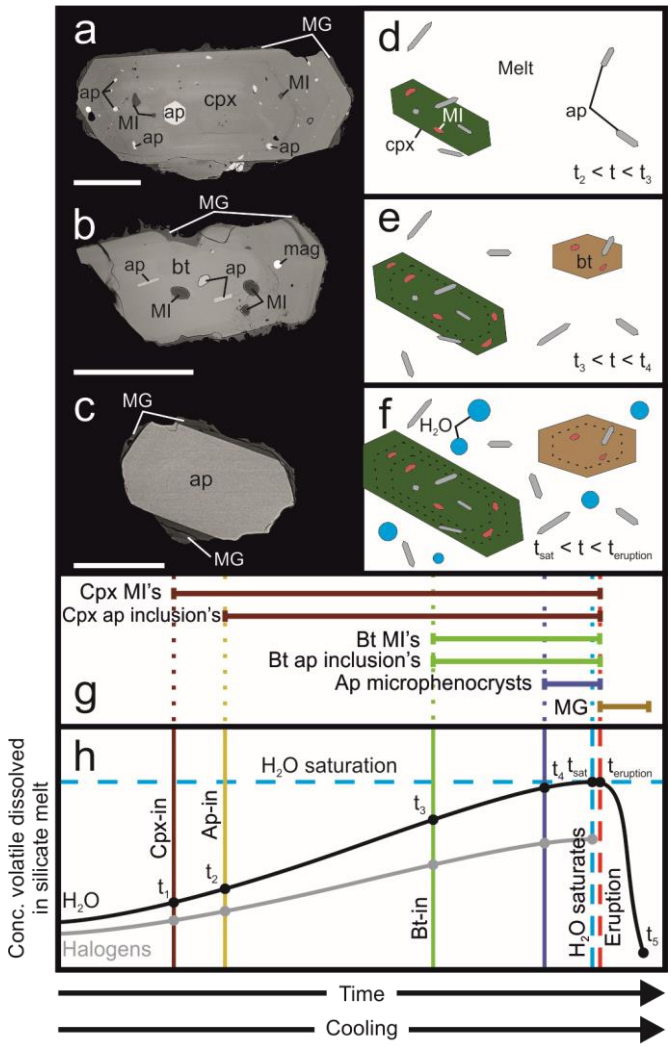

Figure 1 | Textural relations of hydrous phases in the Astroni 1 magma. a–c, Backscattered-electron (BSE) images showing clinopyroxene (cpx, **a**) and biotite (bt, **b**) phenocrysts, and an apatite microphenocryst (ap, **c**). **d–g**, Sketches show how progressive mineral growth and entrapment of inclusions may capture the magmatic volatile evolution through time, during cooling (**g**). t_1–t_5 refer to events in **h**, such as the onset of crystallization of selected mineral phases (cpx-in, ap-in and bt-in). t_4 represents the timescale after which apatite microphenocryst compositions may be preserved. **h**, Sketch showing the evolution of H_2O and halogens during volatile-undersaturated, isobaric crystallization. During vapour-saturated crystallization, H_2O is buffered in the melt and F/Cl increases. Scale bars, **a**—250 μm, **b**—500 μm; **c**—100 μm. Mag, magnetite; MI, melt inclusion; MG, matrix glass.

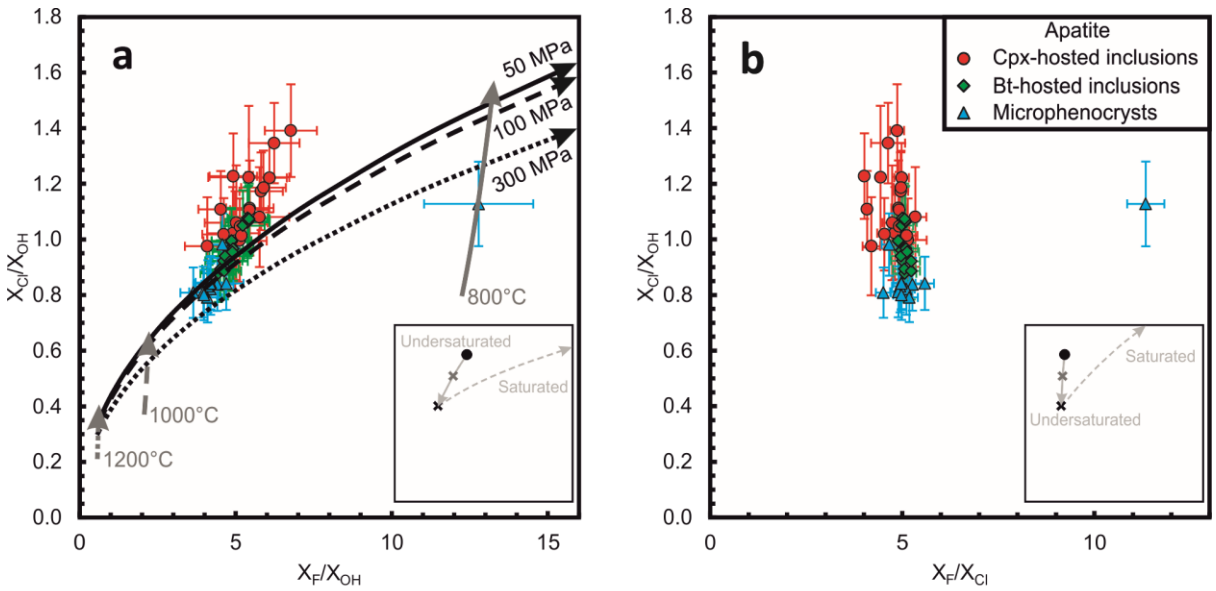

Figure 2 | Volatile compositions of Astroni 1 apatites. a Apatite volatile compositions in X_F/X_{OH} versus X_{Cl}/X_{OH} space. Arrows show modelled compositional trajectories[12] at a constant melt composition, with decreasing temperature (1,200–700 °C) under isobaric conditions (50, 100, 300 MPa; black arrows) and decreasing pressure (1,000–0 MPa) under isothermal conditions (800, 1,000 and 1,200 °C; grey arrows). **b** Apatite volatile compositions in X_F/X_{Cl} versus X_{Cl}/X_{OH} space. Insets show compositional trajectories during volatile-undersaturated (solid line) and volatile-saturated (dashed line) crystallization[33]. Apatite crystallization begins at the black point, *biotite-in* is after 40% crystallization (grey cross) and volatile saturation occurs after 73% crystallization (black cross). See Supplementary Discussion for model details. Errors bars represent precision with a 90% confidence interval. Data are distinguished on the basis of their textural association (see legend).

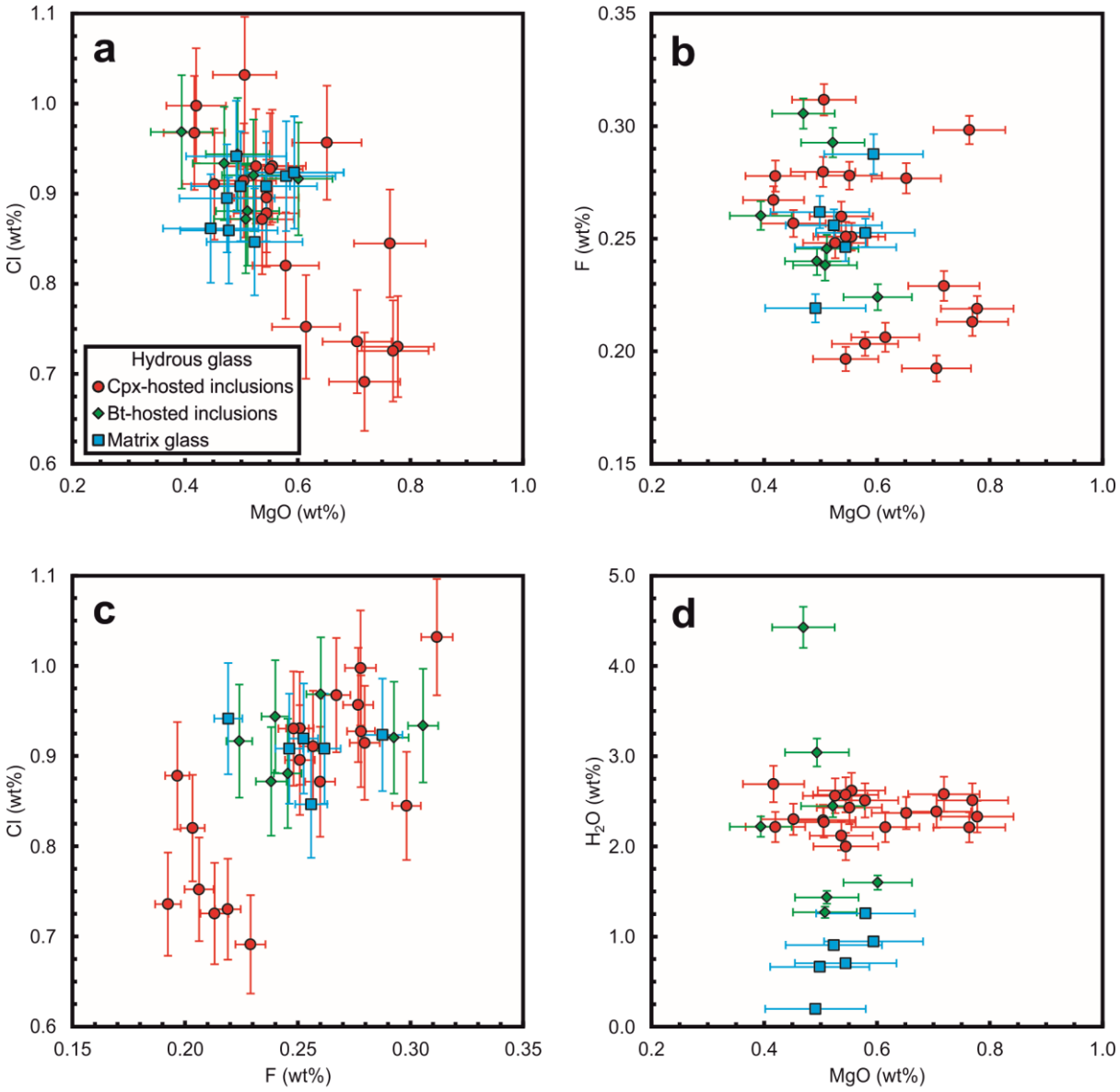

Figure 3 | The volatile contents of Astroni 1 hydrous glasses. a,**b**, MgO versus Cl and F, respectively. **c**, F versus Cl. **d**, MgO versus H_2O. MgO and Cl were measured by EPMA. F and H_2O were measured by SIMS. Error bars represent precision with ±1 s.d. (EPMA data) and a 90% confidence interval (SIMS data). Data are distinguished on the basis of their textural association (see legend).

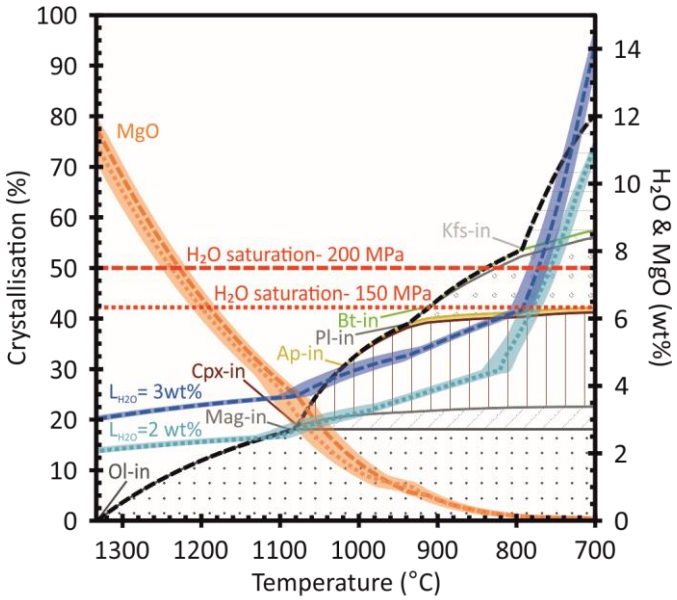

Figure 4 | Rhyolite-MELTS thermodynamic model for Astroni 1. Summary of mineral phase proportions and extent of crystallization (black dashed line) at 150 MPa and L_{H2O} = 3 wt% for a cooling and crystallizing Astroni 1 magma. Residual melt MgO (orange) and H_2O (blue) are shown at 150 MPa, L_{H2O} = 2 wt% (dotted lines) and 3 wt% (dashed lines), and L_{H2O} = 2–3 wt%, 50–300 MPa (coloured fields). Red lines show typical H_2O solubility in phonolitic melts at 150 and 200 MPa (refs 21,32). Volatile saturation is not predicted until *T* ≈ 800 °C; after clinopyroxene (cpx, vertical lines), apatite (ap), plagioclase (pl, spots) and biotite (bt, diagonal lines) have all joined the crystallizing assemblage. Additional symbols: Ol, olivine (black dots); mag, magnetite (diagonal lines); Kfs, K-feldspar (horizontal lines).